THE JOURNAL OF PHYSICAL CHEMISTRY Letters

Letter

pubs.acs.org/JPCL

2D H-Bond Network as the Topmost Skin to the Air−Water Interface

Simone Pezzotti,* Daria Ruth Galimberti, and Marie-Pierre Gaigeot*

LAMBE CNRS UMR8587, Laboratoire Analyse et Modélisation pour la Biologie et l'Environnement, Université d'Evry val d'Essonne, Boulevard F. Mitterrand, Bat Maupertuis, 91025 Evry, France

Université Paris-Saclay, 91190 Saint-Aubin, France

ABSTRACT: We provide a detailed description of the structure of water at the interface with the air (liquid−vapor LV interface) from state-of-the-art DFT-based molecular dynamics simulations. For the first time, a two-dimensional (2D) H-bond extended network has been identified and fully characterized, demonstrating that interfacial water is organized into a 2D sheet with H-bonds oriented parallel to the instantaneous surface and following its spatial and temporal oscillations. By analyzing the nonlinear vSFG (vibrational sum frequency generation) spectrum of the LV interface in terms of layer-by-layer signal, we demonstrate that the 2D water sheet is solely responsible for the spectral signatures, hence providing the interfacial 3.5 Å thickness effectively probed in nonlinear interfacial spectroscopy. The 2D H-bond network unraveled here is the essential key to rationalize macroscopic properties of water−air interfaces, as demonstrated here for spectroscopy and the surface potential.

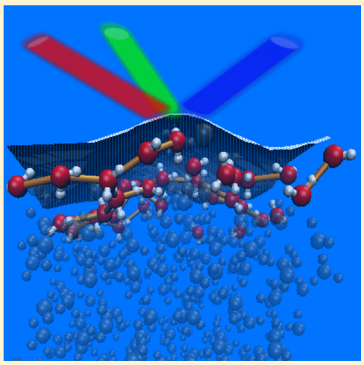

The structure of liquid water at the interface with air plays a key role in the chemistry of water droplets, of primary interest in atmospheric science because many relevant atmospheric chemical reactions take place at the surface of sea spray particles.[1−4] These reactions occur with different mechanisms, rates, and time scales from the ones in bulk liquid water,[5−9] and such differences can be rationalized only through characterization of the structure adopted by water at the interface.

The structure of water at the interface with the vapor phase (LV interface) has up-to-now been mainly characterized through nonlinear vibrational sum frequency generation (vSFG) spectroscopy,[10−23] recording the nonlinear second-order susceptibility $\chi^{(2)}(\omega)$ as a function of frequency ω. Phase-resolved vSFG provides direct measurements of the real $\Re(\chi^{(2)}(\omega))$ and imaginary $\Im(\chi^{(2)}(\omega))$ parts of the susceptibility,[13,15,20] whose signs provide knowledge of the average orientation of the water molecules at the interface. For precise and detailed characterization of the interfacial water structural organization, coupling vSFG experiments to theoretical modeling by molecular dynamics (MD) simulations has been essential as one can directly follow the evolution with time of the microscopic arrangement of the water molecules and extract the associated vSFG signal from the dynamics.[24] Such coupling has been achieved in the literature by various flavors of MD, with classical force fields,[25−29] possibly supplemented by nuclear quantum corrections,[25] mixed classical and quantum dynamics[30,31] with only a few O−H/O−D vibrational oscillators quantum mechanically represented, and ab initio DFT-based molecular dynamics.[32,33] Others have characterized the interfacial structure without calculating vSFG signals; see, for instance, refs 34−39.

A large understanding of the interfacial water structure has hence been obtained by coupling vSFG experiments and MD simulations, although the actual spatial structural organization and the H-bonding network are still debated.[25,38] Another recent hot and controversial debate has agitated the experimental[15,20] and theoretician communities[24,25,31,33] regarding the intensity and structural origin of the $\Im(\chi^{(2)}(\omega))$ signal for frequencies ω < 3200 cm^{-1}. The latest consensus is that there might be a tiny positive feature recorded below 3170 cm^{-1}, whose intensity is much weaker than that measured earlier.[13,15,20] Shen et al. further suggest that this feature is unrelated to surface resonance and therefore unrelated to the interfacial water structure,[20] while Morita et al. attributed it to surface water dimerization inducing charge transfer and dipole anisotropy.[24]

From experimental and theoretical works in the literature, the general consensus is that the 3700 cm^{-1} positive band in $\Im(\chi^{(2)}(\omega))$ arises from dangling O−H oscillators pointing toward the vacuum, while the 3200−3400 cm^{-1} negative broad band is due to H-bonded water molecules with O−H oscillators pointing, on average, toward the liquid phase.[21,24] Isotopic dilution (experiments and simulations) has furthermore shown that the 3200 cm^{-1} sub-band disappears for HOD, therefore revealing inter- and intramolecular water couplings.[21] Morita and collaborators have shown the existence of water dimers being responsible for the positive band <3100 cm^{-1} in the initial vSFG experiment[11] due to the anisotropy of dipoles in such conformations.[21,28] Khune et al.[38] added more detailed structural information using the Willard and Chandler instantaneous surface,[39] hence revealing well-defined water layers. Their structural picture of the air−water interface is that

Received: May 19, 2017
Accepted: June 22, 2017
Published: June 22, 2017

DOI: 10.1021/acs.jpclett.7b01257
J. Phys. Chem. Lett. 2017, 8, 3133−3141

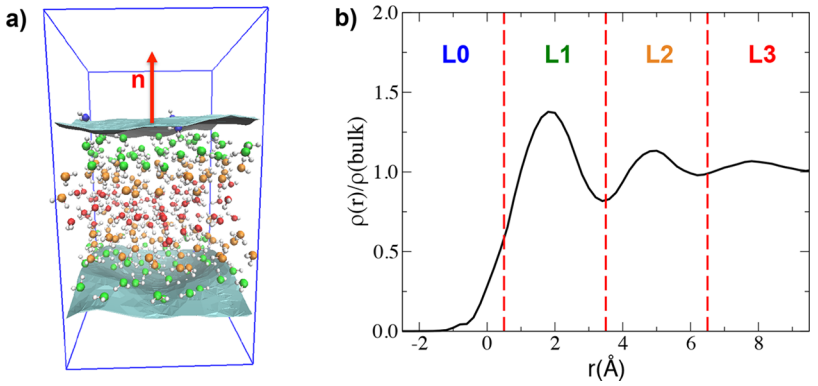

Figure 1. Water layers. (a) Snapshot from the DFT-MD simulation representing the instantaneous surface in light blue and the different water layers (L0 in blue, L1 in green, L2 in orange, L3 in red) identified and discussed in the text. The red arrow $\vec{n}$ represents the normal to the surface, defined from the liquid to vapor phase. (b) Time-averaged water density normalized with respect to bulk liquid water. The density is plotted as a function of the distance from the instantaneous surface. The distance is defined as positive in the liquid phase and negative in the vapor phase. The different water layers are identified by dashed vertical lines and labeled L0−L3.

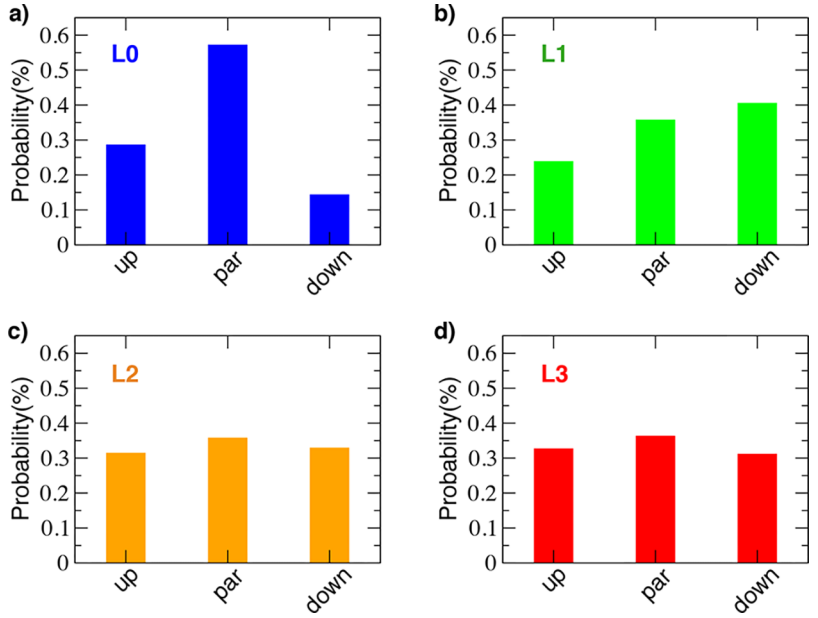

Figure 2. Water orientation: probability (%) for each water molecule in each identified water layer (L0−L3, Figure 1) to be oriented with its dipole moment pointing toward the vacuum (up), parallel to the interface (par), or toward the bulk of water (down). See the Computational details section for more information on these definitions. The direction used for the normal to the surface is shown in Figure 1.

the topmost layer is dominated by waters with one O−H dangling toward the vapor while simultaneously being involved as a H-bond (HB) acceptor and donor with the layer just below. In this second layer, water molecules are reversely oriented with one O−H at least pointing toward the liquid phase, but this layer also includes water molecules that are oriented parallel to the surface, that is, with their O−H oscillators contained within the (instantaneous) surface plane. These latter were shown to serve for interlayer and strong intralayer H-bonding. For the first time, Kuhne et al. inferred that the air−water interface is structurally ordered within ∼5 Å thickness. In their remarkable work, Paesani et al.[25] obtained striking agreement between calculated and experimental vSFG spectra using their developed many-body potential, showing in particular that the (positive) low-frequency band does not exist. Their dissection of the vSFG features into structural organization is solely done in terms of many-body interactions and nuclear quantum effects, especially showing three-body interactions to be pivotal. Beyond the "dangling water molecules", the structural assignment of the interface given in ref 25 is that, on average, interfacial water molecules are made of tetrahedral waters (∼35% of the waters within 3.2 Å from the instantaneous surface) and doubly H-bonded waters simultaneously acting as the donor and acceptor (∼18% of the waters within 3.2 Å from the surface). No mention of the actual thickness responsible for the vSFG spectrum is given, nor an explicit 3D view of the interfacial HB network within the water layers. In their initial[40] and revised works,[31] Skinner et al. interpreted the vSFG spectrum in terms of pairs of water molecules being the HB donor and acceptor, each water being classified by the total number of HBs formed in the pair (4−0) and by how many of those are H-atom donors (N, none; S, single; D, double). They hence showed that pairs of type 4_D−2_S, 2_S−4_D, 4_D−4_D, and 3_D−4_D are responsible for the vSFG spectrum, and depending on the force field and frequency map parametrizations in their works, the 4_D−2_S HBs between two

DOI: 10.1021/acs.jpclett.7b01257
J. Phys. Chem. Lett. 2017, 8, 3133−3141

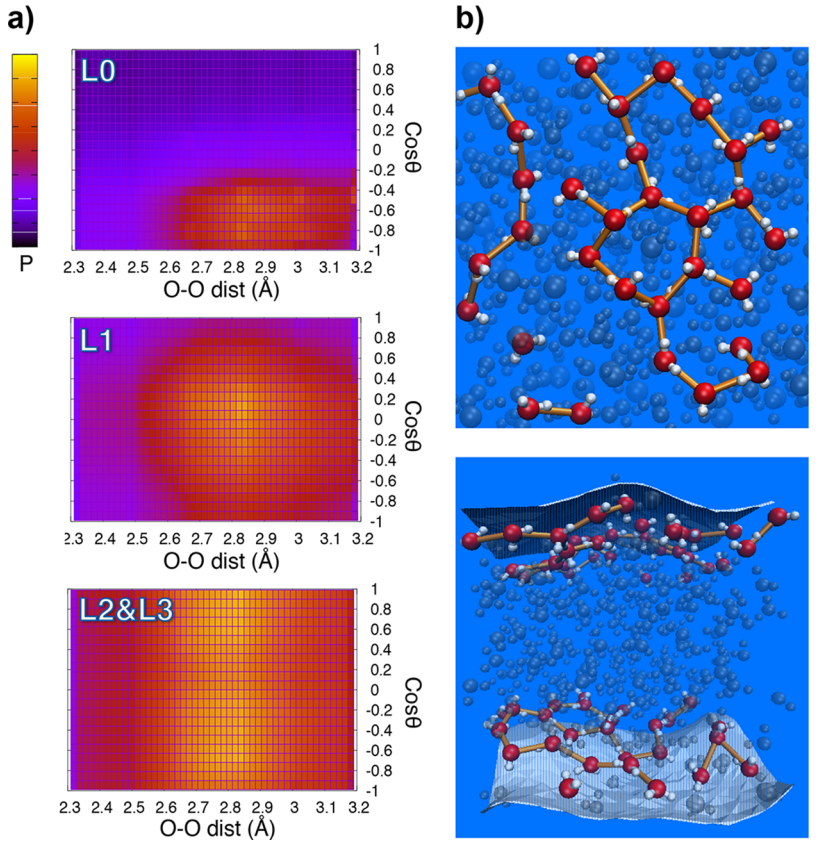

Figure 3. (a) 3D plots of the HB patterns formed between the water molecules located in layers L0, L1, and L2−L3. The horizontal axis represents the O−O distance (Å) between 2 H-bonded water molecules, and the vertical axis provides the angle (cosine value) between the O−O vector (from donor to acceptor) and the normal to the surface (oriented from the liquid to vapor phase). The colors represent the probability (P) to find one O−H group forming one HB with a given distance and orientation. The probability increases from blue to yellow. (b) Snapshot from the simulations showing the 2D network in L1, top view (top) and side view (bottom). The water molecules involved in the structures are highlighted with respect to the other molecules, and the HBs within the plane are drawn in orange. The instantaneous surface is shown by the white colored areas in the side view.

water molecules were shown to be responsible for the <3100 cm^{-1} vSFG band. The latest parametrizations[31] show a cancellation of this positive band by negative contributions from 4_D−4_D HBs, thus providing no final band in this domain, as in Tahara's experiment.[15] No demonstration of the actual thickness responsible for the vSFG spectrum is given in these works, and no systematic 3D structural organization (e.g., in layers) is given beyond the pairs description above. With a crude geometric definition of interfacial layers of water and a small simulation box, we have previously shown[32] that a very thin layer of 2−3 Å is responsible for the vSFG signal. No precise structural organization of the water molecules within this thickness was given beyond the orientation of the water dipole moments and their relation to the positive and negative vSFG bands in the imaginary $\chi^{(2)}(\omega)$.

By carefully defining the interfacial layers with the instantaneous surface method[39] and their structural organization (orientation of water molecules and the HB network in space) and by calculating the $\chi^{(2)}(\omega)$ susceptibility as a function of these layers, we provide here an in-depth description of the water structural organization into well-defined layers of water at the liquid−air interface and into well-defined H-bonding networks, which are used to calculate $\chi^{(2)}(\omega)$ signatures layer by layer. This in turn allows us to give a precise definition of the liquid interface thickness effectively probed before centrosymmetry takes over. We especially demonstrate for the first time that the air−water vSFG signal arises from a thin sheet of water (3.5 Å thickness) organized in a 2D collective and extended H-bonded network with the HBs being oriented parallel to the instantaneous surface. Such structural organization will certainly be of utmost importance once (in)organic molecules and/or ions are accommodated at the interface, as would be the case for water droplets in atmospheric conditions.

We have performed density functional theory-based MD simulations (DFT-MD) on a liquid phase composed of 256 water molecules in contact with vapor represented by vacuum (see the Computational Methods section). See the snapshot in Figure 1a. In order to fully rationalize the molecular structures at the liquid water−vapor (LV) interface and the vSFG signal arising from such organization, we evaluate the evolution of water structural properties as a function of the distance from the surface. The LV boundary is modeled using the instantaneous surface defined by Willard and Chandler,[39] which takes into account the fluctuations in time and space of the topmost molecules' positions. With such a definition of the interface, the density of water along the perpendicular direction to the surface is well-defined.[39] Water layers can hence be identified, as illustrated by the vertical dotted lines in Figure 1b. By evaluating the water density (Figure 1b), the orientation of the water molecules (Figure 2), and the HB network as a function of water molecules belonging to the identified layers (see the Computational Methods section for details), it is

DOI: 10.1021/acs.jpclett.7b01257
J. Phys. Chem. Lett. 2017, 8, 3133−3141

possible to unambiguously define four distinct water layers in our simulation box, with different structural organizations. These layers are hereafter labeled L0, L1, L2, and L3, as illustrated in Figure 1b.

The present layers definition is in agreement with previous works on the LV interface, in which the instantaneous surface[39] has also been used.[25,38,39] Note that this layering cannot be defined using the average surface based on the Gibbs dividing surface, which neglects the instantaneous fluctuations.[38,39]

Layers L1 and L2 are found with a thickness of 3 Å each (roughly one water monolayer; see illustrations in Figure 1a with water molecules colored in green and orange), layer L3 includes all of the water molecules located farther than 6 Å from the surface (water molecules colored in red in Figure 1a), and L0 includes only the few rare topmost water molecules (within 0.5 Å from the surface) lying just above layer L1 (water molecules colored in blue in Figure 1a). Despite L0 and L1 layers possibly being merged and hence considered as one single topmost water layer (as, e.g., in ref 38), we will maintain the L0/L1 distinction because the water molecules in L0 have distinct structural properties from the waters in the L1 layer, as shown below.

In L0, the water molecules form on average 1.7 HBs, leading to a water density that is half of the value from bulk water (Figure 1b). We remind the reference of an average 3.4 HBs formed in liquid water,[41,42] also reproduced in this work from a simulation of bulk liquid water at room temperature applying the same electronic DFT-MD setup as that for the LV interface. The waters in L0 are mainly oriented with their dipole moment pointing toward the vacuum (29% of the molecules) or parallel to the instantaneous surface (58%), as shown in Figure 2a. They systematically have one dangling O−H pointing toward the vapor. On the contrary, a change in the net orientation of the water molecules is observed in layer L1 (0.5−3.5 Å from the surface), with 40% of the molecules with their dipole moment now pointing toward the bulk phase (i.e., "down", Figure 2b). This layer is also characterized by a higher density than that in bulk water (Figure 1b) and an average number of HBs per molecule of 2.9. Such structural characterization of layers L0 and L1 does not depart from previous theoretical works at different levels of theory, sizes, and time scales.[38,39]

For all of the investigated structural properties (density, HB, dipole orientation), layers L0 and L1 thus differ significantly from bulk liquid water, where in particular both an average number of HBs of 3.4 and random orientations are found. These two conditions start to be satisfied only after a 3.5 Å distance from the surface, in layers L2 and L3 (Figure 2c,d). Bulk structural conditions are therefore reached in these layers, and centrosymmetry would thus be expected, as strikingly confirmed in Figure 5c,d with our vSFG theoretical signals for these two layers (discussed in detail below).

The water molecules in L0 are found never H-bonded between themselves (on average); they systematically have one dangling O−H pointing toward the vapor phase and the other O−H mostly H-bonded to molecules located in L1. If the molecular structure of L0 is easily deduced from the analyzed properties and well characterized in the literature (e.g., refs 21, 25, 38, and 39), the same is not true for L1, where a clear picture of the molecular arrangement leading to the specific properties observed here (higher density, undercoordination, net down orientation) is still lacking.

To get this detailed picture, Figure 3a presents 3D plots where the probability for the water molecules in each layer to form HBs with a given O−O distance and given orientation with respect to the normal to the surface is evaluated. We hence clearly demonstrate that, while the water molecules located in L0 form rather long HBs with orientations toward L1 (cosines lower than −0.4) and while the waters in L2−L3 form a homogeneous HB network with 2.65−2.85 Å distances and all possible orientations in space (cosines homogeneously distributed from −1 to +1), a very distinct preferential orientation of the water−water HBs is observed in L1, with cosine values mainly distributed within ±0.2, that is, O−H···O HBs parallel to the (instantaneous) surface. The number and type of HBs made by the interfacial water molecules have been discussed in theoretical works in the literature by Morita et al.[21] who described water dimers and by Skinner et al.[31,40] and Pasesani et al.[25] who discussed 4_D, 3_D, and 2_S pairs of waters. Khune et al.[38] also found water molecules oriented with their O−H bonds parallel to the surface, capable of making interlayer bridges and intralayer HBs. In all of these works, there is however no clear quantitative description of whether these HBs are restricted to water pairs or to other more complex extended structures.

An interfacial collective and extended HB network in layer L1 (and *only* in layer L1) is unraveled and described here for the first time. Our results indeed demonstrate that the water structure in L1 is more than the mere existence of water pairs, and instead, L1 is organized into an extended network of HBs oriented parallel to the surface (see above), connecting ∼70% of the water molecules in the layer. To show this, we have analyzed the intermolecular structures adopted by the water molecules located in L1 (see the Computational Methods section). We find that, on average, only 8% of the molecules form dimers, 18% form small chains/rings (of size <7), and the rest of the water molecules in L1 form one single extended H-bonded structure with the HB network located within a plane parallel to the instantaneous surface. Snapshots from the simulations highlighting this water network are shown in Figure 3b. From the top view, it is clear that the vast majority of the water molecules located in L1 is organized into one single extended structure (that we will call "the 2D network"). The side view shows that the 2D network is comprised within a thin sheet, the network of HBs being oriented in the plane parallel to the instantaneous surface, with the 2D water sheet following the oscillations of the instantaneous surface.

The water molecules in the sheet form on average 1.7 HBs (over a total of 2.9) oriented parallel to the surface and contributing to the 2D network; each water systematically forms one HB as a donor and one as an acceptor with two molecules located within the same monolayer. The number of such HBs (1.7) is higher than the average number of 0.8, obtained for molecules belonging to a similarly defined monolayer of the same thickness cut through the liquid. Also noteworthy, the 2D water sheet is composed of water molecules forming more in-plane HBs than in the bulk (1.7 vs 0.8) despite a lower total number of HBs per water (2.9 vs 3.4 in bulk), and the HBs are of similar strength as in the bulk (see O···O distances in Figure 3). In total, taking the nomenclature from Skinner et al.,[40] the 2D network is composed of water molecules being 3_D (forming two HBs as the donor and one as the acceptor, 44% of the population), 4_D (two HBs as the donor and two as the acceptor, 24%), and 2_S (one HB as the donor and one as the acceptor, 22%). These are indeed the populations from Skinner's works, and the novelty

DOI: 10.1021/acs.jpclett.7b01257
J. Phys. Chem. Lett. 2017, 8, 3133−3141

shown here is that these waters give rise to a collective and extended 2D H-bonded network, as depicted in Figure 3b.

We are now in the position to rationalize the maximum observed in the density profile in layer L1 (Figure 1); it is due to the existence of the 2D water sheet and its accompanying higher number of intralayer HBs formed within the 2D network. In a similar way, also the net down orientation of water molecules obtained in L1 (Figure 2b) can now be explained thanks to the 2D network. The water molecules in the sheet systematically have one O−H oriented parallel to the surface and contributing to the 2D HB network, while the other O−H mostly points down toward layer L2 because there is a higher probability to form HBs with water molecules in L2 than in L0, where there is less than half of the bulk water density. Because of this preferential dipole orientation in L1, there is a net total dipole thus present at the interface that leads to a positive electric field oriented along the normal to the surface (average extracted from the current simulation; see the Computational Methods section). Integrating the field, a surface electric potential of 0.1 V is obtained, in rather good agreement with the experimental value of 0.1−0.2 V.[43] This theoretical value matches better the experiment than our previous work (0.47 V)[32] because of the increased size of the simulation box providing a better statistical representation. We can thus provide a molecular explanation for the surface potential of water at the interface with air, being the consequence of the net dipole induced in the water sheet by the 2D HB network.

In the same way, also the nonlinear vSFG spectrum of the water−air interface can now be fully interpreted in terms of the interfacial structures just characterized.

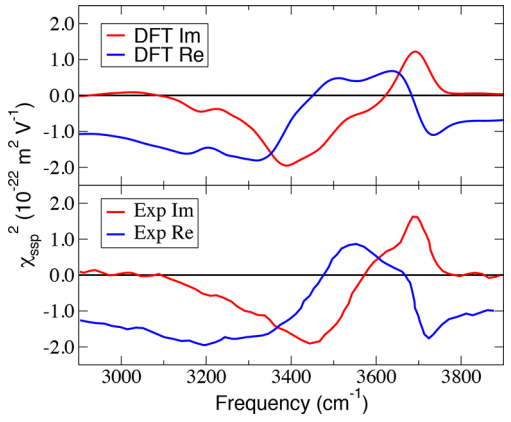

Figure 4. Top panel: Calculated phase-resolved *ssp*-vSFG spectrum for the water LV interface in the O−H stretching region: real part of $\chi^{(2)}$ in blue, imaginary part of $\chi^{(2)}$ in red. Bottom panel: Recent HD-SFG spectrum from Tahara's group:[15] real part of $\chi^{(2)}$ in blue, imaginary part of $\chi^{(2)}$ in red. Note the absolute intensities being reported in the calculated spectra.

Figure 4 gives in the top panel the theoretical imaginary $\Im(\chi^{(2)})$ and real $\Re(\chi^{(2)})$ parts of the nonlinear $\chi^{(2)}(\omega)$ susceptibility calculated in the present work using the time-dependent formalism initially introduced by Morita et al.[29,44]

$$\chi_{ssp}^{(2)}(\omega) = \frac{-\mathrm{i}}{k_B T \omega} \sum_{i=1}^{N_W} \int_0^\infty \mathrm{d}t \, \exp(\mathrm{i}\omega t) \langle \dot{\alpha}_{ss}^i(t) \dot{p}_p^i(0) \rangle \quad (1)$$

with the *ssp* signal calculated here, where $s = x,y$ and $p = z$; $\dot{p}_z^i$ and $\dot{\alpha}_{xx}^i$ ($\dot{\alpha}_{yy}^i$) are, respectively, components of the time derivative of the dipole moment and polarizability tensor of the individual water molecules (the sum runs over N_W water molecules). See the Computational Methods section for all of the computational details. Note also that the theoretical spectra report absolute intensities directly comparable to the experimental ones. The imaginary and real parts of the $\chi^{(2)}(\omega)$ theoretical vSFG signal nicely compare with the experiments from Shen et al.[20] and Tahara et al.[15] (Figure 4, bottom panel), correctly reproducing the positions of the main peaks (i.e., 3695 and 3395 cm^{-1} for $\Im(\chi^{(2)})$, 3730 and 3565 cm^{-1} for $\Re(\chi^{(2)})$), and the changes in sign (i.e., 3605 and 3110 cm^{-1} for $\Im(\chi^{(2)})$; 3690 and 3455 cm^{-1} for $\Re(\chi^{(2)})$). Theoretical band positions are within 20−50 cm^{-1} of the experiments. Moreover, the comparison with the experiments from Tahara's group shows how our calculation reproduces for the first time the correct absolute intensities of all of the main peaks in both $\Im(\chi^{(2)})$ and $\Re(\chi^{(2)})$ and especially the maximum of the negative band in the $\Im(\chi^{(2)})$ signal due to the H-bonded O−H oscillators. This is one more indication of the validity of the water structure given by our DFT-MD simulation.

Let us further quantify the agreement between simulated and experimental spectra by calculating "band intensities" defined by the integration of each given active band. Intensities are important to discuss as they take into account band shapes that reflect the quality of structure, dynamics, and inter- and intramolecular couplings. Hence, integrating the negative band of the spectrum obtained from our DFT-MD simulation, we obtain a vSFG intensity of -4.44×10^{-20} m^2V^{-1} to be compared to -4.44×10^{-20} m^2V^{-1} in the experiment and $+1.21 \times 10^{-20}$ m^2V^{-1} (simulation) vs $+1.44 \times 10^{-20}$ m^2V^{-1} (experiment) for the positive band. Both intensities show very good to excellent agreement between calculation and experiment. There is however a 15% intensity missing in the positive band of the theoretical spectrum, which is due to the 3600 cm^{-1} missing shoulder. According to ref 45, this shoulder is due to intramolecular couplings within water molecules having two free O−H oscillators, which can be found in layer L0 only and very rarely, that is, 20% of the water molecules located in L0 (numbers from the present work). Although the associated signal does exist in our spectrum for layer L0 (see dissection below with spectral contribution layer/layer, Figure 5), it is a tiny shoulder that is washed away once other layers contributions are added up.

To interpret and dissect the vSFG signal at the molecular level, we calculate individual spectra for each single layer and rationalize the total spectrum of the water−air interface in terms of the different signatures provided by each layer. Figure 5 shows the imaginary and real parts of $\chi^{(2)}(\omega)$ calculated separately for layers L0, L1, L2, and L3, with the signal normalized per number of water molecules located within each layer for the sake of clarity.

The vSFG activity strongly decreases with the increase in the distance from the surface, becoming zero in layers L2 and L3, where centrosymmetry is thus reached. This allows us to give a clear and unambiguous definition of the water LV interface probed by vSFG, which is composed of the molecules belonging to layers L0 and L1, that is, within a thin 3.5 Å distance from the surface. Note that such thickness was already inferred in our previous work based on a smaller simulation box

DOI: 10.1021/acs.jpclett.7b01257
J. Phys. Chem. Lett. 2017, 8, 3133−3141

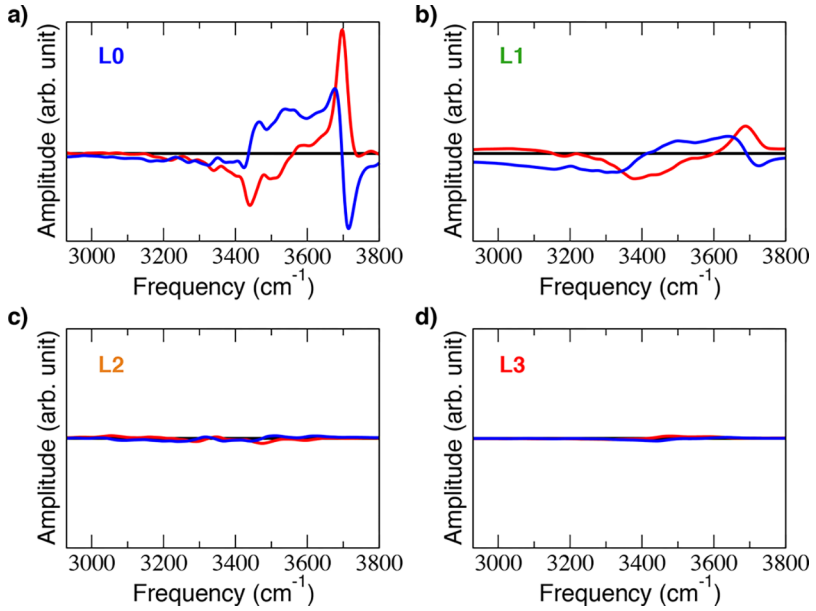

Figure 5. Calculated phase-resolved vSFG spectra ($\Re(\chi^{(2)})$ in blue and $\Im(\chi^{(2)})$ in red) for each identified water layer: L0 (a), L1 (b), L2 (c), and L3 (d). Signals normalized per the number of water molecules located in each layer.

and using a crude definition of the layers.[32] However, we demonstrate here that there is no vSFG signal arising from water located farther than 3.5 Å (L2 and L3). Despite the higher vSFG intensity per molecule seen in L0, only 9% of the LV water population is located in this layer. Consequently, the vSFG signal of the LV interface is dominated by the 2D water sheet unraveled in layer L1.

Both spectra for L0 and L1 water layers show two main bands in the $\Im(\chi^{(2)}(\omega))$: a negative (rather broad) band between 3200 and 3600 cm^{-1} and a positive (rather sharp) peak located at 3700 cm^{-1}. Strikingly, despite the similar vSFG contributions provided by these two layers, the molecular arrangements leading to the spectroscopically active bands in these two signals differ. As already discussed, in L0, the molecules systematically have one O−H group not H-bonded and pointing toward the vacuum and the other H-bonded to molecules in L1; the dangling O−H gives rise to the SFG positive sharp peak at 3700 cm^{-1}, while the second H-bonded O−H gives rise to the negative 3200−3600 cm^{-1} band. The broadness of the latter is due to the inhomogeneous environment offered for the H-bonding. The structure in L1 is characterized by the 2D network unraveled here; the molecules have one O−H oriented parallel to the surface and contributing to the intralayer 2D HB network, while the other O−H mostly points down toward layer L2; the stretching of the O−H groups pointing parallel to the surface is not active in the *ssp*-vSFG spectrum, while the stretching of the second O−H groups oriented perpendicular to the surface is vSFG-active. As the majority of these O−H groups (2/3) are H-bonded to water molecules located in L2, they thus provide the negative band in the $\Im(\chi^{(2)})$, while when they are not H-bonded and point upward along the normal to the surface (1/3 of the oscillators) they provide the positive peak at 3700 cm^{-1}. This peak is less intense than that in L0 as there are far fewer such oscillators contributing in L1.

To conclude, we comment on the very small positive intensity of the vSFG signal below 3200 cm^{-1} arising solely from layer L1. The presence of this positive band has been highly debated in the past few years, with the 2015−2016 latest experiments from Tahara and Shen groups[15,20] pointing to no such peak[15] or to a very tiny peak[20] (whose feature might not even be related to the interfacial water structure[20]). Our theoretical $\Im\chi^{(2)}(\omega)$ has a very small positive amplitude (Figure 4), so small that it does not allow us to provide final conclusions regarding its effective presence (or not) in the spectrum of the water LV interface. However, we can conclude that if this signal is indeed present, it arises *only* from the water molecules located in layer L1, belonging to the 2D water sheet because all of the other layers provide no intensity in this region (Figure 5). It would therefore have a structural origin. To go further, we have extracted cluster conformations from the 2D water sheet in L1, and we have calculated the harmonic IR and Raman spectra of these clusters. Both IR and Raman show active modes below 3200 cm^{-1}. The eigenvectors of these modes show the collective motions of the O−H groups involved in the 2D HB network unraveled in this work. This result is in line with previous theoretical works[24,31] where the signal in the lower-frequency domain is shown related to intermolecular couplings. Skinner et al.[31,40] have demonstrated, in particular, that the vibrational modes giving a signal in this frequency region are due to intermolecular couplings between 3_D, 4_D, and 2_S water molecules, which we now know to be the ingredients of the 2D network in the L1 layer solely responsible for the air−water vSFG signal.

In conclusion, we have characterized the molecular arrangement at the water LV interface in terms of the specific structures formed by water in the different layers below the surface. Coherently with previous works,[38,39] a higher water density than that in the bulk, a net water dipole moment orientation, and undercoordination of water molecules have been observed at the interface. We have demonstrated for the first time that all of these particular structural properties derive from a specific extended water structure, which dominates the molecular arrangement at the interface; a 2D HB network within 3.5 Å thickness (L1 layer in the text), giving rise to a 2D interfacial water sheet, has indeed been unraveled here. This 2D

DOI: 10.1021/acs.jpclett.7b01257
J. Phys. Chem. Lett. 2017, 8, 3133−3141

network is built upon an average of ∼70% of the interfacial water molecules, connected by a collective and extended net of HBs oriented parallel to the instantaneous surface. With the knowledge of such a 2D network, we have furthermore been able to rationalize the positive value measured for the surface potential of water at the interface with air, as well as the microscopic structures at the origin of the HD-vSFG signal at the water−air interface.

In order to interpret the HD-vSFG spectral signatures, we have presented a new methodology based on evaluation of the spectroscopic signatures of the different identified water layers. Calculating the vSFG spectra from each layer separately, we have been able to demonstrate that no signal is coming from water layers located farther than 3.5 Å from the surface, thus definitely providing the thickness probed in vSFG experiments at the air−water interface. Note that this result confirms the early view from Morita and Hynes[44] of the topmost layer contributing to the free O−H vSFG peak and few supplementray water layers contributing to the H-bonded band. Here we have not only quantified the interface thickness but have also provided a detailed structural description of the underlying 2D H-bonded network. Strikingly, HD-vSFG spectroscopy is partly blind to the specific orientation of the O−H oscillators parallel to the instantaneous surface as these are not SFG-active. What HD-vSFG does measure in the 2D water sheet is the signature of the rest of the O−H oscillators not engaged in the 2D network, giving rise to the positive peak for the few free O−H molecules or to the negative band for the O−H molecules that are pointing downward and are H-bonded to the next water layer. This latter layer is not vSFG-active anymore because of structural centrosymmetry being recovered.

The methodology introduced here represents an advance in the interpretation of vSFG spectra of aqueous interfaces, directly linking the molecular structures in the different water layers to their respective spectroscopic signatures and providing interfacial thicknesses effectively probed in nonlinear vSFG spectroscopies. The 2D interfacial water sheet unraveled here is the essential key to rationalize macroscopic properties of water−air interfaces, as shown here for spectroscopy and the surface potential, and paves the way to more general links between structure and macroscopic properties (e.g., surface tension). Also, the unusual Pockels effect measured at the air−water interface by Suzuki et al.[46] under a field applied parallel to the interface could be due to the interfacial 2D network ordering. We also trust that this 2D network will have consequences on how/where electrolytes and (in)organic molecules can be accommodated at the air−water interface.

COMPUTATIONAL METHODS

DFT-based molecular dynamics simulations (DFT-MD) have been carried out with the CP2K package,[47,48] consisting of Born−Oppenheimer MD, BLYP[49,50] electronic representation including Grimme D2 correction for dispersion,[51,52] GTH pseudopotentials[53] for O and H atoms, and a combined plane-wave (400 Ry density cutoff) and TZV2P basis set. The simulation box of 19.734 × 19.734 × 35 Å^3 is composed of a liquid phase made of 256 water molecules, periodically repeated in the x and y directions and separated by a vacuum layer of 15 Å from the replica in the vertical z direction. The classical Newton's equations of motion for the nuclei are integrated through the Verlet algorithm and a time step of 0.4 fs. After an equilibration period of 5 ps (*NVE* ensemble with possible rescaling of velocities followed by a pure *NVE* ensemble), the system was simulated for 20 ps in the *NVE* ensemble, with an average temperature of 315 K.

Our DFT-MD simulations have shown to be able not only to reproduce the intensity ratio between the main bands of the vSFG spectra but also to predict the correct absolute band intensities (and band positions within 20−50 cm^{-1} of the experiment). The excellent agreement between calculated and experimental spectra proves that the chosen level of theory and the dimension of the box are a good compromise in accuracy for reproducing the physical properties of the system (structural and vibrational) at an acceptable computational cost. The vSFG signal, related to the resonant electric dipole nonlinear susceptibility $\chi^{(2)}(\omega)$, as well as its real and imaginary components, has been calculated following the time-dependent method introduced by Morita et al.[29,44]

$$\chi_{PQR}^{(2)}(\omega) = \frac{-\mathrm{i}}{k_\mathrm{b}T\omega}\int_0^\infty \mathrm{d}t\ \exp(\mathrm{i}\omega t)\langle \dot{A}_{PQ}(t)\dot{M}_R(0)\rangle \tag{2}$$

where $\dot{A}_{PQ}(t)$ and $\dot{M}_R(0)$ are, respectively, the time derivative of the components of the total polarizability tensor and total dipole moment, (P,Q,R) are any x, y, z direction in the laboratory frame, and k_b and T are the Boltzmann constant and temperature of the simulated system. $\langle\cdots\rangle$ is a time correlation function. Following the model proposed by Khatib et al.,[54] supposing that at the frequencies of interest only the OH stretching motions are contributing, the total dipole moment and polarizability tensor can be decomposed at each time t along the trajectory into individual O−H bond contributions ($\dot{\alpha}_{PQ}(t)$ and $\dot{\mu}_R(0)$), with the following equations

$$\dot{A}_{PQ} = \sum_{m=1}^{M}\sum_{n=1}^{N_\mathrm{m}} \dot{\alpha}_{mn,PQ}(t) \tag{3}$$

$$\dot{M}_R = \sum_{m=1}^{M}\sum_{n=1}^{N_\mathrm{m}} \dot{\mu}_{mn,R}(t) \tag{4}$$

where M and N_m are, respectively, the number of water molecules and O−H oscillators per molecule.

Using the direction cosine matrix (D) projecting the molecular frame (x, y, z) onto the laboratory frame (P, Q, R) and assuming that the O−H stretching is much faster than the modes involving a bond reorientation, the following expressions for the molecular dipole moment and polarizability tensor components are obtained

$$\dot{\alpha}_{PQ}(t) \simeq \sum_{i}^{x,y,z}\sum_{j}^{x,y,z} D_{Pi}(t)D_{Qj}(t)\frac{\mathrm{d}\alpha_{ij}}{\mathrm{d}r_z}v_z(t) \tag{5}$$

$$\dot{\mu}_R(t) \simeq \sum_{i}^{x,y,z} D_{Ri}(t)\frac{\mathrm{d}\mu_i}{\mathrm{d}r_z}v_z(t) \tag{6}$$

The D matrix and the projection of the velocities on the O−H bond axis (v_z) can be readily obtained from the DFT-MD trajectory, while $\frac{\mathrm{d}\alpha_{ij}}{\mathrm{d}r_z}$ and $\frac{\mathrm{d}\mu_i}{\mathrm{d}r_z}$ can be parametrized. Parameterization from refs 54 and 55 has been used.

Analyses of the DFT-MD trajectory into instantaneous surface and water layers (Figure 1) follow the derivation by Willard and Chandler,[39] the analyses into water−water HBs use the definitions from Galli and co-workers[41] with O(−H)···O ≤ 3.2 Å and the O−H···O angle in the range of [140−220]°, and

DOI: 10.1021/acs.jpclett.7b01257
J. Phys. Chem. Lett. 2017, 8, 3133−3141

analyses of the water dipole orientations (Figure 2) are done by projecting the HOH bisector onto the normal to the surface, providing a measure denoted d_z. Three orientation classes are defined: "up" for $d_z \geq 0.33$, "down" for $d_z \leq -0.33$, and "parallel" ("par") for $-0.33 < d_z < 0.33$. Note that different cutoffs than 0.33 have been tested for this classification, providing the same trends and same conclusions.

The 2D HB network unraveled here in the water sheet in L1 has been characterized by evaluating the probability to form intralayer HBs for each water molecule of L1 with respect to a water molecule belonging to a layer defined with the same thickness randomly extracted from the bulk liquid. The preferential planar orientation for the 2D HB network found in layer L1 has been obtained by evaluating the orientation distribution of the H-bonded O−H groups in each layer with respect to the normal to the surface. The identification of dimers, clusters, and sheet structures in L1 has been done with a connected component analysis and considering two water molecules H-bonded together if they satisfy Galli's criteria (see above) for more than 70% of the simulation time.

For orientational and spectroscopic calculations, the vector normal to the LV surface is taken oriented toward the vacuum, as illustrated in Figure 1.

The electric field at the air−water interface $\boldsymbol{E}(z)$ has been obtained fully ab initio from the optimized electronic wave function and the positions of the nuclei, at a given time along the trajectory, using the standard routine implemented in the CP2K[47,48] package. $\boldsymbol{E}(z)$ has been calculated each 100 fs and then averaged over these sampled points. The electric potential has been calculated by integrating $\boldsymbol{E}(z)$ along the z direction, $\phi = \int_{z_a}^{\infty} \mathrm{d}z \cdot \boldsymbol{E}(z)$. The theoretical value of 0.1 V obtained here is in excellent agreement with the experimental value of 0.1−0.2 V.[43] This is a further demonstration that the chosen computational setup is able to well describe chemical and physical properties of the system.

AUTHOR INFORMATION

Corresponding Authors

*E-mail: simone.pezzotti@univ-evry.fr (S.P.).
*E-mail: mgaigeot@univ-evry.fr (M.-P.G.).

ORCID

Marie-Pierre Gaigeot: 0000-0002-3409-5824

Notes

The authors declare no competing financial interest.

ACKNOWLEDGMENTS

This work was performed under Grant ANR DYNAWIN ANR-14-CE35-0011-01. This work was performed using HPC resources from GENCI-France Grant 072484 (CINES/IDRIS/Curie).

REFERENCES

(1) Laskin, A.; Gaspar, D. J.; Wang, W.; Hunt, S. W.; Cowin, J. P.; Colson, S. D.; Finlayson-Pitts, B. J. Reactions at Interfaces as a Source of Sulfate Formation in Sea Salt Particles. *Science* **2003**, *301*, 340−344.

(2) Finlayson-Pitts, B. J.; Pitts, J. N. *Chemistry of the Upper and Lower Atmosphere*; Academic Press, 2000.

(3) Finlayson-Pitts, B. J. Atmospheric Chemistry. *Proc. Natl. Acad. Sci. U. S. A.* **2010**, *107*, 6566−6567.

(4) Dawson, M.; Varner, M. E.; Perraud, V.; Ezell, M. J.; Gerber, R. B.; Finlayson-Pitts, B. J. Simplified Mechanism for New Particle Formation from Methane Sulfonic Acid, Amines, and Water via Experiments and Ab Initio Calculations. *Proc. Natl. Acad. Sci. U. S. A.* **2012**, *109*, 18719−18724.

(5) Knipping, E. M.; Lakin, M. J.; Foster, K. L.; Jungwirth, P.; Tobias, D. J.; Gerber, R. B.; Dabdub, D.; Finlayson-Pitts, B. J. Experiments and Simulations of Ion-Enhanced Interfacial Chemistry on Aqueous NaCl Aerosols. *Science* **2000**, *288*, 301−306.

(6) Katrib, Y.; Deiber, G.; Schweitzer, F.; Mirabel, P.; George, C. Chemical Transformation of Bromine Chloride at the Air/Water Interface. *J. Aerosol Sci.* **2001**, *32*, 893−911.

(7) Clifford, D.; Donaldson, D. J. Direct Experimental Evidence for a Heterogeneous Reaction of Ozone with Bromide at the Air- Aqueous Interface. *J. Phys. Chem. A* **2007**, *111*, 9809−9814.

(8) Laskin, A.; Wang, H.; Robertson, W. H.; Cowin, J. P.; Ezell, M. J.; Finlayson-Pitts, B. J. A New Approach to Determining Gas-Particle Reaction Probabilities and Application to the Heterogeneous Reaction of Deliquesced Sodium Chloride Particles with Gas-Phase Hydroxyl Radicals. *J. Phys. Chem. A* **2006**, *110*, 10619−10627.

(9) Graham, J. D.; Roberts, J. T.; Anderson, L. D.; Grassian, V. H. The 367 nm PhotoChemistry of OClO Thin Films and OClO Adsorbed on Ice. *J. Phys. Chem.* **1996**, *100*, 19551−19558.

(10) Shen, Y. R. Surface Properties Probed by Second-Harmonic and Sum-Frequency Generation. *Nature* **1989**, *337*, 519−525.

(11) Du, Q.; Freysz, E.; Shen, Y. R.; Superfine, R. Vibrational Spectroscopy of Water at the Vapor/Water Interface. *Phys. Rev. Lett.* **1993**, *70*, 2313−2316.

(12) Du, Q.; Freysz, E.; Shen, Y. R. Surface Vibrational Spectroscopic Studies of Hydrogen Bonding and Hydrophobicity. *Science* **1994**, *264*, 826−828.

(13) Ji, N.; Ostroverkhov, V.; Tian, C. S.; Shen, Y. R. Characterization of Vibrational Resonances of Water-Vapor Interfaces by Phase-Sensitive Sum-Frequency Spectroscopy. *Phys. Rev. Lett.* **2008**, *100*, 096102.

(14) Shen, Y. R.; Ostroverkhov, V. Sum-Frequency Vibrational Spectroscopy on Water Interfaces:Polar Orientation of Water Molecules at Interfaces. *Chem. Rev.* **2006**, *106*, 1140−1154.

(15) Nihonyanagi, S.; Kusaka, R.; Inoue, K.; Adhikari, A.; Yamaguchi, S.; Tahara, T. Accurate Determination of Complex $\chi^{(2)}$ Spectrum of the Air/Water Interface. *J. Chem. Phys.* **2015**, *143*, 124707.

(16) Sovago, M.; Campen, R. K.; Wurpel, G. W. H.; Muller, M.; Bakker, H. J.; Bonn, M. Vibrational Response of Hydrogen-Bonded Interfacial Water is Dominated by Intramolecular Coupling. *Phys. Rev. Lett.* **2008**, *100*, 173901.

(17) Nihonyanagi, S.; Ishiyama, T.; Lee, T.; Yamaguchi, S.; Bonn, M.; Morita, A.; Tahara, T. Unified Molecular View of the Air/Water Interface Based on Experimental and Theoretical Spectra of an Isotopically Diluted Water Surface. *J. Am. Chem. Soc.* **2011**, *133*, 16875−16880.

(18) Zhang, Z.; Piatkowski, L.; Bakker, H.; Bonn, M. Ultrafast Vibrational Energy Transfer at the Water/Air Interface Revealed by Two-Dimensional Surface Vibrational Spectroscopy. *Nat. Chem.* **2011**, *3*, 888−893.

(19) Inoue, K.; Ishiyama, T.; Nihonyanagi, S.; Yamaguchi, S.; Morita, A.; Tahara, T. Efficient Spectral Diffusion at the Air/Water Interface Revealed by Femtosecond Time-Resolved Heterodyne-Detected Vibrational Sum Frequency Generation Spectroscopy. *J. Phys. Chem. Lett.* **2016**, *7*, 1811−1815.

(20) Sun, S.; Liang, R.; Xu, X.; Zhu, H.; Shen, Y. R.; Tian, C. Phase Reference in Phase-Sensitive Sum-Frequency Vibrational Spectroscopy. *J. Chem. Phys.* **2016**, *144*, 244711.

(21) Ishiyama, T.; Imamura, T.; Morita, A. Theoretical Studies of Structures and Vibrational Sum Frequency Generation Spectra at Aqueous Interfaces. *Chem. Rev.* **2014**, *114*, 8447−8470.

(22) Hsieh, C.-S.; Okuno, M.; Hunger, J.; Backus, E. H. G.; Nagata, Y.; Bonn, M. Aqueous Heterogeneity at the Air/Water Interface Revealed by 2D-HD-SFG Spectroscopy. *Angew. Chem., Int. Ed.* **2014**, *53*, 8146−8149.

(23) Chen, X.; Hua, W.; Allen, H. C.; Huang, Z. Interfacial Water Structure Associated with Phospholipid Membranes Studied by Phase-

DOI: 10.1021/acs.jpclett.7b01257
J. Phys. Chem. Lett. 2017, 8, 3133−3141

Sensitive Vibrational Sum Frequency Generation Spectroscopy. *J. Am. Chem. Soc.* **2010**, *132*, 11336−11342.
(24) Ishiyama, T.; Morita, A. Computational Analysis of Vibrational Sum Frequency Generation Spectroscopy. *Annu. Rev. Phys. Chem.* **2017**, *68*, 355−377.
(25) Medders, G. R.; Paesani, F. Dissecting the Molecular Structure of the Air/Water Interface from Quantum Simulations of the Sum-Frequency Generation Spectrum. *J. Am. Chem. Soc.* **2016**, *138*, 3912−3919.
(26) Byrnes, S. J.; Geissler, P. L.; Shen, Y. R. Ambiguities in Surface Nonlinear Spectroscopy Calculations. *Chem. Phys. Lett.* **2011**, *516*, 115−124.
(27) Perry, A.; Neipert, C.; Kasprzyk, C. R.; Green, T.; Space, B.; Moore, P. B. A Theoretical Description of the Polarization Dependence of the Sum Frequency Generation Spectroscopy of the Water/Vapor Interface. *J. Chem. Phys.* **2005**, *123*, 144705.
(28) Ishiyama, T.; Morita, A. Vibrational Spectroscopic Response of Intermolecular Orientational Correlation at the Water Surface. *J. Phys. Chem. C* **2009**, *113*, 16299−16302.
(29) Morita, A.; Ishiyama, T. Recent Progress in Theoretical Analysis of Vibrational Sum Frequency Generation Spectroscopy. *Phys. Chem. Chem. Phys.* **2008**, *10*, 5801−5816.
(30) Auer, B. M.; Skinner, J. L. Vibrational Sum-Frequency Spectroscopy of the Water Liquid/Vapor Interface. *J. Phys. Chem. B* **2009**, *113*, 4125−4130.
(31) Ni, Y.; Skinner, J. L. Communication: Vibrational Sum-Frequency Spectrum of the Air-Water Interface, Revisited. *J. Chem. Phys.* **2016**, *145*, 031103.
(32) Sulpizi, M.; Salanne, M.; Sprik, M.; Gaigeot, M.-P. Vibrational Sum Frequency Generation Spectroscopy of the Water Liquid Vapor Interface from Density Functional Theory-Based Molecular Dynamics Simulations. *J. Phys. Chem. Lett.* **2013**, *4*, 83−87.
(33) Ohto, T.; Usui, K.; Hasegawa, T.; Bonn, M.; Nagata, Y. Toward Ab Initio Molecular Dynamics Modeling for Sum-Frequency Generation Spectra; an Efficient Algorithm Based on Surface-Specific Velocity-Velocity Correlation Function. *J. Chem. Phys.* **2015**, *143*, 124702.
(34) Buch, V. J. Molecular Structure and OH-Stretch Spectra of Liquid Water Surface. *J. Phys. Chem. B* **2005**, *109*, 17771−17774.
(35) Mucha, M.; Frigato, T.; Levering, L. M.; Allen, H. C.; Tobias, D. J.; Dang, L.; Jungwirth, P. J. Unified Molecular Picture of the Surfaces of Aqueous Acid, Base, and Salt Solutions. *J. Phys. Chem. B* **2005**, *109*, 7617−7623.
(36) Dang, L. X.; Chang, T.-M. Molecular Dynamics Study of Water Clusters, Liquid, and Liquid−Vapor Interface of Water with Many-Body Potentials. *J. Chem. Phys.* **1997**, *106*, 8149.
(37) Benjamin, I. Vibrational Spectrum of Water at the Liquid/Vapor Interface. *Phys. Rev. Lett.* **1994**, *73*, 2083−2086.
(38) Kessler, J.; Elgabarty, H.; Spura, T.; Karhan, K.; Partovi-Azar, P.; Hassanali, A. A.; Kuhne, T. D. Structure and Dynamics of the Instantaneous Water/Vapor Interface Revisited by Path-Integral and Ab Initio Molecular Dynamics Simulations. *J. Phys. Chem. B* **2015**, *119*, 10079−10086.
(39) Willard, A.; Chandler, D. Instantaneous Liquid Interfaces. *J. Phys. Chem. B* **2010**, *114*, 1954−1958.
(40) Tainter, C.; Ni, Y.; Shi, L.; Skinner, J. L. Hydrogen Bonding and OH-Stretch Spectroscopy in Water: Hexamer (Cage), Liquid Surface, Liquid, and Ice. *J. Phys. Chem. Lett.* **2013**, *4*, 12−17.
(41) White, J. A.; Schwegler, E.; Galli, G.; Gygi, F. The Solvation of Na^+ in Water: First-Principles Simulations. *J. Chem. Phys.* **2000**, *113*, 4668−4673.
(42) Pfeiffer-Laplaud, M.; Gaigeot, M. Adsorption of Singly Charged Ions at the Hydroxylated (0001) α-Quartz/Water Interface. *J. Phys. Chem. C* **2016**, *120*, 4866−4880.
(43) Fawcett, W. The Ionic Work Function and its Role in Estimating Absolute Electrode Potentials. *Langmuir* **2008**, *24*, 9868−9875.
(44) Morita, A.; Hynes, J. T. A Theoretical Analysis of the SFG Spectrum of the Water Surface. II- Time Dependent Approach. *J. Phys. Chem. B* **2002**, *106*, 673−685.
(45) Schaefer, J.; Backus, E.; Nagata, Y.; Bonn, M. Both Inter- and Intramolecular Coupling of O-H Groups Determine the Vibrational Response of the Water/Air Interface. *J. Phys. Chem. Lett.* **2016**, *7*, 4591−4595.
(46) Suzuki, Y.; Osawa, K.; Yukita, S.; Kobayashi, T.; Tokunaga, E. Anomalously Large Electro-Optic Pockels Effect at the Air-Water Interface with an Electric Field Applied Parallel to the Interface. *Appl. Phys. Lett.* **2016**, *108*, 191103.
(47) Hutter, J.; Iannuzzi, M.; Schiffmann, F.; VandeVondele, J. CP2K: Atomistic Simulations of Condensed Matter Systems. *WIREs Comput. Mol. Sci.* **2014**, *4*, 15−25.
(48) VandeVondele, J.; Krack, M.; Mohamed, F.; Parrinello, M.; Chassaing, T.; Hutter, J. Quickstep: Fast and Accurate Density Functional Calculations Using a Mixed Gaussian and Plane Waves Approach. *Comput. Phys. Commun.* **2005**, *167*, 103−128.
(49) Becke, A. D. Density-Functional Exchange-Energy Approximation with Correct Asymptotic Behavior. *Phys. Rev. A: At., Mol., Opt. Phys.* **1988**, *38*, 3098−3100.
(50) Lee, C.; Yang, W.; Parr, R. G. Development of the Colle-Salvetti Correlation-Energy Formula into a Functional of the Electron Density. *Phys. Rev. B: Condens. Matter Mater. Phys.* **1988**, *37*, 785−789.
(51) Grimme, S. Accurate Description of van der Waals Complexes by Density Functional Theory Including Empirical Corrections. *J. Comput. Chem.* **2004**, *25*, 1463−1473.
(52) Grimme, S. Semiempirical GGA-Type Density Functional Constructed with a Long-Range Dispersion Correction. *J. Comput. Chem.* **2006**, *27*, 1787−1799.
(53) Goedecker, S.; Teter, M.; Hutter, J. Separable Dual-Space Gaussian Pseudopotentials. *Phys. Rev. B: Condens. Matter Mater. Phys.* **1996**, *54*, 1703−1710.
(54) Khatib, R.; Backus, E. H. G.; Bonn, M.; Perez-Haro, M.-J.; Gaigeot, M.-P.; Sulpizi, M. Water Orientation and Hydrogen-Bond Structure at the Fluorite/Water Interface. *Sci. Rep.* **2016**, *6*, 24287.
(55) Corcelli, S. A.; Skinner, J. L. Infrared and Raman Line Shapes of Dilute HOD in Liquid H_2O and D_2O from 10 to 90 C. *J. Phys. Chem. A* **2005**, *109*, 6154−6165.

DOI: 10.1021/acs.jpclett.7b01257
J. Phys. Chem. Lett. 2017, 8, 3133−3141